J. Fluid Mech. (2020), *vol.* 889, A16. © Beijing University of Aeronautics and Astronautics, 2020. Published by Cambridge University Press
doi:10.1017/jfm.2020.89

Falling film with insoluble surfactants: effects of surface elasticity and surface viscosities

Tao Hu[1], **Qingfei Fu**[1,2] **and Lijun Yang**[1,2,†]

[1]School of Astronautics, Beihang University, 100083 Beijing, China

[2]Beijing Advanced Innovation Center for Big Data-Based Precision Medicine, Beihang University, 100083 Beijing, China

(Received 8 August 2019; revised 10 November 2019; accepted 24 January 2020)

The stability of a thin falling film with both surface elasticity and surface viscosities induced by insoluble surfactants on its free surface is studied. Based on the full Navier–Stokes equations and surfactant concentration equation with corresponding boundary conditions, a weighted residual model (WRM) is derived to investigate the long-wave instability of the thin film incorporating the influence of surfactants. The Chebyshev spectral collocation method is employed to solve the linear stability of the film. The results show good agreement between the WRM and full equations. It is found that surface elasticity decreases the temporal growth rate and increases the critical Reynolds number, showing a stabilizing impact on the film. And the surface viscosity effect slightly reduces the growth rate and cutoff wavenumber while it does not alter the critical Reynolds number. Nonlinear travelling wave solutions are obtained using the WRM equations. As the surface elasticity is enhanced, the speed of travelling waves gradually approaches the corresponding linear neutral value, implying that the dispersion effect is damped; and the amplitudes of both fast waves and slow waves are suppressed by surface elasticity. Moreover, the bifurcation diagram of travelling waves is influenced by the surface viscosity, which basically promotes the speed of travelling waves with relatively large wavelengths. As the surface viscosity effect becomes stronger, for fast waves the amplitude of the humps slightly increases while that of the troughs becomes smaller for slow waves.

Key words: thin films

1. Introduction

Falling liquid films have received much attention from researchers in recent decades (Chang 1994; Oron, Davis & Bankoff 1997; Weinstein & Ruschak 2004; Craster & Matar 2009; Ruyer-Quil *et al.* 2014). As examples of open-flow systems, they are encountered in many industrial fields, like coating processes (Alekseenko, Nakoryakov & Pokusaev 1994), heat exchangers (Salvagnini & Taqueda 2004), cooling microelectronic devices (Squires & Quake 2005), chemical reactors (Bender, Stephan & Gambaryan-Roisman 2017), food processing and thermal protection design

†Email address for correspondence: yanglijun@buaa.edu.cn

of combustion chambers in rocket engines (Shine & Nidhi 2018). Investigation of this subject was pioneered by the experimental work of Kapitza & Kapitza (1949). Theoretical studies were later carried out by Benjamin (1957) and Yih (1963), where the threshold value of Reynolds number when the film is unstable with long-wave perturbations was shown to depend on the inclination angle. Alekseenko, Nakoryakov & Pokusaev (1985) experimentally measured the growth rate of the waves and compared that with theoretical results. Smith (1990) carefully scrutinized the mechanism of this long-wave instability and concluded that the inertial stress associated with the Reynolds number is the key factor that destabilizes the film. Later, Liu, Paul & Gollub (1993) conducted decisive experiments and confirmed the theoretical predictions of the critical Reynolds number of Benjamin (1957) and Yih (1963). Over the years, experimental efforts have been made continually to validate and complement the theoretical studies on falling films (Liu, Schneider & Gollub 1995; Alekseenko *et al.* 2005; Kharlamov *et al.* 2015; Adebayo *et al.* 2017; Charogiannis *et al.* 2017; Charogiannis & Markides 2019).

Since the full treatment of the Navier–Stokes equations together with boundary conditions on the free surface and solid bottom remains a cumbersome task, many efforts have been made to seek a simplified model based on the long-wave nature of the film instability. Benney (1966) first devised a single evolution equation of the film thickness h using an expansion method in a small film parameter. Following this procedure, a number of researches have been performed that showed its effectiveness in the prediction of the instability threshold (Lin 1974; Joo, Davis & Bankoff 1991; Sadiq & Usha 2008; Samanta 2008; Ogden, Pascal & D'Alessio 2011; Dávalos-Orozco 2012). However, several authors have pointed out that the Benney-type equation blows up and yields unphysical solutions at moderate Reynolds numbers (Pumir, Manneville & Pomeau 1983; Scheid *et al.* 2005). On the other hand, an integral-boundary-layer (IBL) model was first developed by Shkadov (1967) which couples the film thickness h and local flow rate q. Then, a weighted residual technique was proposed which is able to remove the inconsistency between the original IBL model and the full Navier–Stokes equations in determining the instability threshold (Ruyer-Quil & Manneville 2000, 2002). After that, this method has been adopted to model the film flow in many other situations (Trevelyan *et al.* 2007; Samanta, Ruyer-Quil & Goyeau 2011; Amaouche, Djema & Ait Abderrahmane 2012; Ruyer-Quil, Chakraborty & Dandapat 2012; Ding & Wong 2015; D'Alessio & Pascal 2016; Ellaban, Pascal & D'Alessio 2017; Fu, Hu & Yang 2018).

Surfactants could be used to induce a variation in surface tension (known as Marangoni effect or surface elasticity) and surface viscosity, which can thus adjust the surface dynamics (Scriven & Sternling 1960). The influence of insoluble surfactants on a falling film was first studied theoretically by Benjamin (1964) and Whitaker (1964). They both found an increase of the critical Reynolds number when surface elasticity is included, concluding that there was a stabilizing effect of surfactants, which was qualitatively in accordance with several earlier experimental observations (Emmert 1954; Stirba & Hurt 1955; Tailby & Portalski 1961). Blyth & Pozrikidis (2004) identified a new Marangoni mode when surfactants are present and concluded that there was a stabilizing effect of surfactants overall. Using a perturbation expansion method, Oron & Edwards (1993) derived a nonlinear evolution equation for the free-surface displacement of the film in the presence of interfacial viscous stress. Pereira & Kalliadasis (2008) considered the problem in both linear and nonlinear regimes. They solved the Orr–Sommerfeld eigenvalue problem of the full equations and obtained three different modes in linear instability, where they stated that the

Marangoni stress caused by surfactants reduces the domain of film instability. On the basis of the weighted residual model (WRM), they also found that the amplitude and velocity of travelling waves on the film are decreased by the Marangoni effect. Ji & Setterwall (1994) studied the case where surfactants are soluble and volatile, which they claimed is necessary to destabilize the Marangoni mode.

Karapetsas & Bontozoglou (2014) focused on the influence of arbitrary solubility of the surfactants and found that the interfacial concentration gradient decreases with increasing surfactant solubility; higher-order calculations showed that the speed of adsorption/desorption at the interface plays a role at finite wavelength. Meanwhile, experiments were also carried out where an attenuation influence of soluble surfactants on inlet disturbances were observed (Georgantaki, Vlachogiannis & Bontozoglou 2012, 2016). In some recent relative research, Bhat & Samanta (2018) considered a falling film down a slippery plane in the presence of insoluble surfactants and showed that insoluble surfactants stabilize the shear mode at high Reynolds number. Also, they found that when the Péclet number exceeds its critical value, the surfactant mode becomes unstable, while the inertia force does not affect the surfactant mode significantly (Bhat & Samanta 2019). Pascal, D'Alessio & Ellaban (2019) developed a model accounting for the transport of surfactants between the surface and the bulk of the film layer where the variation of the fluid density was also incorporated. Their results depict a non-monotonic relation between the critical Reynolds number and the variation of density.

In this paper we study the effect of insoluble surfactants on a falling film when both surface elasticity and surface viscosities are taken into account, which has not been clearly clarified in the literature up to now. Next, § 2 gives the governing equations of the film flow and derives a WRM which accounts for the effects of both surface elasticity and surface viscosities. In § 3, we examine the linear stability characteristics and compare the results of full equations and the WRM. Travelling wave solutions are discussed in § 4, and finally we summarize the main conclusions in § 5.

2. Problem formulation

2.1. *Governing equations*

We consider a two-dimensional incompressible liquid film flowing down an inclined plane. As depicted in figure 1, the interface between the film and the ambient gas is covered with insoluble surfactants. A Cartesian coordinate system (x, y) is established so that the x axis is parallel to the solid bottom and points in the downstream direction while y is normal to the bottom and points outwards. The density, viscosity and surface tension of the fluid are ρ, μ and σ, respectively, g is the gravitational acceleration and θ denotes the inclination angle.

In the film layer, we have the continuity and Navier–Stokes equations:

$$\frac{\partial U}{\partial x}+\frac{\partial V}{\partial y}=0, \tag{2.1}$$

$$\rho\left(\frac{\partial U}{\partial t}+U\frac{\partial U}{\partial x}+V\frac{\partial U}{\partial y}\right)=-\frac{\partial P}{\partial x}+\mu\left(\frac{\partial^2 U}{\partial x^2}+\frac{\partial^2 U}{\partial y^2}\right)+\rho g\sin\theta, \tag{2.2}$$

$$\rho\left(\frac{\partial V}{\partial t}+U\frac{\partial V}{\partial x}+V\frac{\partial V}{\partial y}\right)=-\frac{\partial P}{\partial y}+\mu\left(\frac{\partial^2 V}{\partial x^2}+\frac{\partial^2 V}{\partial y^2}\right)-\rho g\cos\theta, \tag{2.3}$$

where U and V are velocity components in the x and y directions, respectively, and P is the pressure. Introducing $F_1=1+(\partial H/\partial x)^2$ and $F_2=1-(\partial H/\partial x)^2$, the

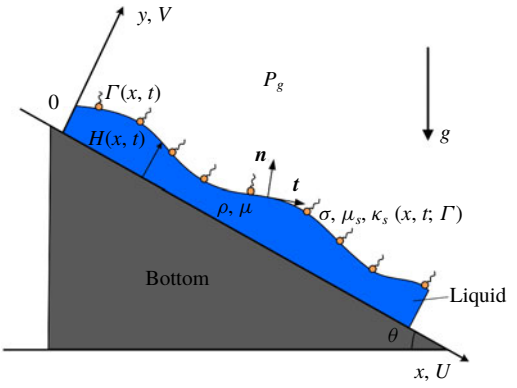

FIGURE 1. Schematic of a thin falling film covered with insoluble surfactants.

concentration Γ of the insoluble surfactants obeys the following transport equation at the interface $y = H(x, t)$ (Pereira & Kalliadasis 2008):

$$\frac{\partial \Gamma}{\partial t} + U\frac{\partial \Gamma}{\partial x} + \frac{\Gamma}{F_1}\left[\left(\frac{\partial U}{\partial x} + \frac{\partial H}{\partial x}\frac{\partial V}{\partial x}\right) + \frac{\partial H}{\partial x}\left(\frac{\partial U}{\partial y} + \frac{\partial H}{\partial x}\frac{\partial V}{\partial y}\right)\right] = \frac{D_s}{\sqrt{F_1}}\frac{\partial}{\partial x}\left(\frac{1}{\sqrt{F_1}}\frac{\partial \Gamma}{\partial x}\right). \tag{2.4}$$

Here the first two terms on the left-hand side of (2.4) denote the material derivative of Γ; while the third term represents the change of the concentration resulting from the stretching of the surface. The term on the right-hand side accounts for the diffusion of surfactants on the surface, with D_s being the surface diffusivity. At the solid bottom $y = 0$, the non-slip boundary condition requires

$$U = V = 0. \tag{2.5}$$

The kinematic condition at the free surface $y = H(x, t)$ is

$$V = \frac{\partial H}{\partial t} + U\frac{\partial H}{\partial x}. \tag{2.6}$$

In the present formulation, we consider the case where the surfactant induces both surface elasticity and viscosities on the free surface. Namely, it not only reduces the surface tension but also induces extra viscous stresses at the interface, as described by Martínez-Calvo & Sevilla (2018), where the free-surface stresses are modelled by two surface viscosities: the surface shear viscosity $\mu_s(\Gamma)$ and dilatational viscosity $\kappa_s(\Gamma)$. Following their procedure, we introduce $\boldsymbol{U}_s = U_n\boldsymbol{n} + U_t\boldsymbol{t}$ to denote the film velocity at the surface with

$$\begin{cases} \boldsymbol{n} = \dfrac{1}{\sqrt{F_1}}\left(-\dfrac{\partial H}{\partial x}, 1\right), \\ \boldsymbol{t} = \dfrac{1}{\sqrt{F_1}}\left(1, \dfrac{\partial H}{\partial x}\right), \end{cases} \quad \text{and} \quad \begin{cases} U_n = \dfrac{1}{\sqrt{F_1}}\left(V - \dfrac{\partial H}{\partial x}U\right), \\ U_t = \dfrac{1}{\sqrt{F_1}}\left(U + \dfrac{\partial H}{\partial x}V\right) \end{cases} \tag{2.7a,b}$$

being the unit normal and tangential vectors and the corresponding velocity components at the surface. If we let $\boldsymbol{T}$ and $\boldsymbol{T}_g$ be the stress tensors of the fluid

and the surrounding gas, respectively, the surface equation of motion is given by (Martínez-Calvo & Sevilla 2018)

$$(\boldsymbol{T}_g - \boldsymbol{T})\cdot\boldsymbol{n} + \nabla_s\sigma - \boldsymbol{n}\cdot(\nabla_s\cdot\boldsymbol{n})\sigma + \nabla_s[(\kappa_s-\mu_s)(\nabla_s\cdot\boldsymbol{U}_s)] \\ -\boldsymbol{n}\cdot(\nabla_s\cdot\boldsymbol{n})(\kappa_s-\mu_s)(\nabla_s\cdot\boldsymbol{U}_s) + \nabla_s\cdot\{\mu_s[(\nabla_s\boldsymbol{U}_s)\cdot\boldsymbol{I}_s + \boldsymbol{I}_s\cdot(\nabla_s\boldsymbol{U}_s)^{\mathrm{T}}]\} = 0, \quad (2.8)$$

where $\boldsymbol{I}_s = \boldsymbol{I} - \boldsymbol{nn}$ is the surface projection operator and $\nabla_s = \boldsymbol{I}_s\cdot\nabla$ is the surface gradient operator, with $\boldsymbol{I}$ being the identity tensor. Note that the pressure of the surrounding gas is assumed to be constant and thus $\boldsymbol{T}_g = -P_g\boldsymbol{I}$. Evaluating the inner product of (2.8) with $\boldsymbol{n}$ and $\boldsymbol{t}$, we obtain two dynamical boundary conditions at $y = H(x, t)$:

$$(P-P_g) - \frac{2\mu}{F_1}\left[\frac{\partial V}{\partial y} + \left(\frac{\partial H}{\partial x}\right)^2\frac{\partial U}{\partial x} - \frac{\partial H}{\partial x}\left(\frac{\partial U}{\partial y} + \frac{\partial V}{\partial x}\right)\right] \\ = -\frac{\partial^2 H}{\partial x^2}\left[\frac{\sigma}{{F_1}^{3/2}} + \frac{1}{{F_1}^2}(\mu_s+\kappa_s)\left(\frac{\partial U_t}{\partial x} - \frac{\partial^2 H}{\partial x^2}\frac{U_n}{F_1}\right)\right] \quad (2.9)$$

and

$$\frac{\mu}{\sqrt{F_1}}\left[\left(\frac{\partial U}{\partial y} + \frac{\partial V}{\partial x}\right)F_2 + 2\frac{\partial H}{\partial x}\left(\frac{\partial V}{\partial y} - \frac{\partial U}{\partial x}\right)\right] \\ = \frac{\partial\sigma}{\partial x} + \frac{\partial}{\partial x}\left[(\mu_s+\kappa_s)\left(\frac{1}{\sqrt{F_1}}\frac{\partial U_t}{\partial x} - \frac{U_n}{{F_1}^{3/2}}\frac{\partial^2 H}{\partial x^2}\right)\right]. \quad (2.10)$$

Here, as noted by Martínez-Calvo & Sevilla (2018), the velocity components U and V in U_t and U_n are interface quantities, which are previously evaluated at the free surface. Considering this fact, for example, the derivative of U with respect to x at the interface is

$$\frac{\partial U(x, y=H(x,t), t)}{\partial x} = \left.\frac{\partial U}{\partial x}\right|_{y=H(x,t)} + \left.\frac{\partial H}{\partial x}\frac{\partial U}{\partial y}\right|_{y=H(x,t)}. \quad (2.11)$$

It is obvious that the two surface viscosities are indistinguishable from each other and act like a single parameter; thus we introduce $\beta = \mu_s + \kappa_s$ to denote the overall effect of surface viscosities for simplicity. Moreover, according to Ponce-Torres *et al.* (2017), the surface viscosities depend on the concentration and can be expressed as $\beta(\Gamma) = \beta^*\Gamma$, with β^* being a surfactant constant. Besides, the surface elasticity represents the surface tension gradient caused by surfactants with the relation $\sigma(\Gamma) = \sigma_0 - \gamma(\Gamma - \Gamma_0)$ (γ being positive here).

We now apply the following scaling procedure to the above equations:

$$\left.\begin{gathered} x = l\bar{x}, \quad y = H_N\bar{y}, \quad U = U_0\bar{u}, \quad V = \delta U_0\bar{v}, \quad H = H_N\bar{h}, \\ t = \frac{l}{U_0}\bar{t}, \quad \Gamma = \Gamma_0\bar{\phi}, \quad P - P_g = \rho U_0^2\bar{p}. \end{gathered}\right\} \quad (2.12)$$

Here H_N is the Nusselt thickness given by

$$H_N = \left(\frac{3\mu Q}{\rho g\sin\theta}\right)^{1/3}, \quad (2.13)$$

where Q is the flow rate, and $U_0 = Q/H_N$ is the average velocity of the basic flow. Note that in (2.12) a thin-film parameter $\delta = H_N/l$ is formulated and $\delta \ll 1$ is considered a small number. After implementing the non-dimensionalization and dropping the bar on the dimensionless variables for convenience, the governing equations (2.1)–(2.10) become

$$\frac{\partial u}{\partial x} + \frac{\partial v}{\partial y} = 0, \tag{2.14}$$

$$\delta Re\left(\frac{\partial u}{\partial t} + u\frac{\partial u}{\partial x} + v\frac{\partial u}{\partial y}\right) = -\delta Re\frac{\partial p}{\partial x} + 3 + \delta^2\frac{\partial^2 u}{\partial x^2} + \frac{\partial^2 u}{\partial y^2}, \tag{2.15}$$

$$\delta^2 Re\left(\frac{\partial v}{\partial t} + u\frac{\partial v}{\partial x} + v\frac{\partial v}{\partial y}\right) = -Re\frac{\partial p}{\partial y} - 3\cot\theta + \delta^3\frac{\partial^2 v}{\partial x^2} + \delta\frac{\partial^2 v}{\partial y^2}, \tag{2.16}$$

$$\begin{aligned}&\frac{\partial \phi}{\partial t} + u\frac{\partial \phi}{\partial x} + \frac{\phi}{f_1}\left[\left(\frac{\partial u}{\partial x} + \delta^2\frac{\partial h}{\partial x}\frac{\partial v}{\partial x}\right) + \frac{\partial h}{\partial x}\left(\frac{\partial u}{\partial y} + \delta^2\frac{\partial h}{\partial x}\frac{\partial v}{\partial y}\right)\right]\\ &\quad = \frac{\delta}{Pe_s\sqrt{f_1}}\frac{\partial}{\partial x}\left(\frac{1}{\sqrt{f_1}}\frac{\partial \phi}{\partial x}\right),\end{aligned} \tag{2.17}$$

where $Re = \rho U_0 H_N/\mu$ is the Reynolds number and $Pe_s = U_0 H_N/D_s$ is the surface Péclet number.

The dimensionless non-slip condition at $y = 0$ is

$$u = v = 0, \tag{2.18}$$

while the kinematic condition at $y = h(x, t)$ can be written as

$$v = \frac{\partial h}{\partial t} + u\frac{\partial h}{\partial x}. \tag{2.19}$$

The dynamic boundary conditions (2.9)–(2.10) are transformed to

$$\begin{aligned}&p - \frac{2\delta}{Ref_1}\left[\frac{\partial v}{\partial y} + \delta^2\left(\frac{\partial h}{\partial x}\right)^2\frac{\partial u}{\partial x} - \frac{\partial h}{\partial x}\left(\frac{\partial u}{\partial y} + \delta^2\frac{\partial v}{\partial x}\right)\right]\\ &\quad = -\frac{\delta}{Re}\frac{\partial^2 h}{\partial x^2}\left[\frac{3\delta[We - Ma(\phi - 1)]}{{f_1}^{3/2}} + \frac{\delta^2 Bo}{{f_1}^2}\phi\left(\frac{\partial u_t}{\partial x} - \delta\frac{\partial^2 h}{\partial x^2}\frac{u_n}{f_1}\right)\right]\end{aligned} \tag{2.20}$$

and

$$\begin{aligned}&\frac{1}{\sqrt{f_1}}\left[\left(\frac{\partial u}{\partial y} + \frac{\partial v}{\partial x}\right)f_2 + 2\delta^2\frac{\partial h}{\partial x}\left(\frac{\partial v}{\partial y} - \frac{\partial u}{\partial x}\right)\right]\\ &\quad = -3\delta Ma\frac{\partial \phi}{\partial x} + \delta^2 Bo\frac{\partial}{\partial x}\left[\phi\left(\frac{1}{\sqrt{f_1}}\frac{\partial u_t}{\partial x} - \frac{\delta u_n}{{f_1}^{3/2}}\frac{\partial^2 h}{\partial x^2}\right)\right],\end{aligned} \tag{2.21}$$

where $We = \sigma_0/\rho g H_N^2 \sin\theta$ is the Weber number, $Ma = \gamma\Gamma_0/\rho g H_N^2 \sin\theta$ denotes the Marangoni number and $Bo = \beta^*\Gamma_0/\mu H_N$ is the Boussinesq number. The other variables are given by

$$u_n = \frac{\delta}{\sqrt{f_1}}\left(v - \frac{\partial h}{\partial x}u\right) \quad \text{and} \quad u_t = \frac{1}{\sqrt{f_1}}\left(u + \frac{\partial h}{\partial x}v\right), \tag{2.22a,b}$$

where

$$f_1 = 1 + \delta^2\left(\frac{\partial h}{\partial x}\right)^2 \quad \text{and} \quad f_2 = 1 - \delta^2\left(\frac{\partial h}{\partial x}\right)^2. \tag{2.23a,b}$$

2.2. *Weighted residual model*

Now we employ the WRM to derive a set of reduced equations that incorporates the effect of insoluble surfactants. As done in previous works (Ogden *et al.* 2011; D'Alessio & Pascal 2016; Ellaban *et al.* 2017; Fu *et al.* 2018), we discard terms of orders higher than $O(\delta^2)$ in (2.14)–(2.21) and begin by assuming a profile of the velocity

$$u = \frac{3q}{2h^3} b_1 + \frac{\delta Ma}{4h} b_2 \frac{\partial \phi}{\partial x}, \tag{2.24}$$

where $b_1 = y(2h - y)$, $b_2 = y(2h - 3y)$ and $q = \int_0^h u \, \mathrm{d}y$ is the flow rate. Note that the prescribed velocity u satisfies the non-slip condition (2.18) and the tangential stress condition (2.21) to the first order in δ:

$$\left.\frac{\partial u}{\partial y}\right|_{y=h} = -3\delta Ma \frac{\partial \phi}{\partial x}. \tag{2.25}$$

Given (2.24), we can readily obtain the velocity v through (2.14) and (2.18). First, equation (2.16) is integrated from $y = h$ to y, combining with the condition (2.20), which yields

$$p = \frac{3\cot\theta}{Re}(h - y) - \frac{\delta}{Re}\left.\frac{\partial u}{\partial x}\right|_h - \frac{\delta}{Re}\frac{\partial u}{\partial x} - \frac{3\delta^2}{Re}[We - Ma(\phi - 1)]\frac{\partial^2 h}{\partial x^2}. \tag{2.26}$$

Equation (2.26) can be used to eliminate the pressure in (2.15) with terms of $O(\delta^2)$ being dropped since p is multiplied with δ in (2.15); while We is assumed to be of $O(1/\delta)$ or larger to retain the effect of surface tension. Integrating (2.14) over the film thickness and applying the conditions (2.18) and (2.19), one arrives at

$$\frac{\partial h}{\partial t} + \frac{\partial q}{\partial x} = 0. \tag{2.27}$$

Here, in accordance with the idea of the Galerkin method, we choose b_1 as the weighted function and multiply it with (2.15), then integrate from $y = 0$ to $y = h$ and utilize (2.21). Moreover, substituting u and v into (2.17) and collecting terms up to $O(\delta^2)$, we finally obtain the following equations for h, q and ϕ:

$$\begin{aligned}
&\frac{\partial q}{\partial t} + \frac{\partial}{\partial x}\left(\frac{9q^2}{7h} + \frac{5\cot\theta}{4Re}h^2 + \frac{15Ma}{4Re}\phi\right) \\
&\quad = \frac{q}{7h}\frac{\partial q}{\partial x} + \frac{5}{2\delta Re}\left(h - \frac{q}{h^2}\right) + \frac{5\delta^2 We}{2Re}h\frac{\partial^3 h}{\partial x^3} \\
&\qquad - \frac{15\delta Bo}{8Reh^2}\left[\phi\frac{\partial}{\partial x}\left(q\frac{\partial h}{\partial x}\right) - h\frac{\partial}{\partial x}\left(\phi\frac{\partial q}{\partial x}\right) + \frac{\partial h}{\partial x}\frac{\partial}{\partial x}(q\phi) - \frac{2q\phi}{h}\left(\frac{\partial h}{\partial x}\right)^2\right] \\
&\qquad + \frac{\delta Ma}{16}\left[h^2\frac{\partial^2\phi}{\partial x\partial t} + \frac{45}{14}hq\frac{\partial^2\phi}{\partial x^2} + \frac{19h}{7}\frac{\partial q}{\partial x}\frac{\partial\phi}{\partial x} + \frac{15q}{7}\frac{\partial h}{\partial x}\frac{\partial\phi}{\partial x}\right] \\
&\qquad + \frac{\delta}{Re}\left[\frac{9}{2}\frac{\partial^2 q}{\partial x^2} - \frac{9}{2h}\frac{\partial q}{\partial x}\frac{\partial h}{\partial x} + \frac{4q}{h^2}\left(\frac{\partial h}{\partial x}\right)^2 - \frac{6q}{h}\frac{\partial^2 h}{\partial x^2}\right],
\end{aligned} \tag{2.28}$$

$$\frac{\partial \phi}{\partial t}+\frac{\partial}{\partial x}\left(\frac{3q\phi}{2h}\right)=\frac{\delta}{Pe_s}\frac{\partial^2\phi}{\partial x^2}+\frac{3\delta Mah}{4}\left[\left(\frac{\partial\phi}{\partial x}\right)^2+\phi\frac{\partial^2\phi}{\partial x^2}\right]+\frac{3\delta Ma\phi}{4}\frac{\partial h}{\partial x}\frac{\partial\phi}{\partial x}-\delta^2\left(\frac{3q}{2h}\frac{\partial^2 h}{\partial x^2}-\frac{\partial^2 q}{\partial x^2}\right)\frac{\partial h}{\partial x}\phi. \tag{2.29}$$

Equations (2.27)–(2.29) constitute a second-order WRM for a falling film with both surface elasticity and surface viscosities induced by the insoluble surfactants on the free surface. In deriving (2.27)–(2.29), it is assumed that the parameters Re, Ma, Bo, Pe_s and $\cot\theta$ are of $O(1)$. By setting $Bo=0$, dropping the second-order terms and using the same scaling, equations (2.27)–(2.29) can recover the first-order weighted IBL equations of Pereira & Kalliadasis (2008) where only the surface elasticity is considered.

3. Linear stability analysis

To study the linear stability of the film, we impose small disturbances on the basic flow, which can be expressed in the form of a normal mode:

$$(h,\,q,\,\phi)=(h_s,\,q_s,\,\phi_s)+(\hat{h},\,\hat{q},\,\hat{\phi})\exp(\mathrm{i}kx+\omega t)+\text{c.c.}, \tag{3.1}$$

where c.c. represents the complex conjugate of the second term. Substituting (3.1) into (2.27)–(2.29) and linearizing the equations, a dispersion relation is obtained as follows:

$$\begin{vmatrix} D_{11} & D_{12} & D_{13} \\ D_{21} & D_{22} & D_{23} \\ D_{31} & D_{32} & D_{33} \end{vmatrix}=0, \tag{3.2}$$

where D_{11}–D_{33} are given by

$$\left.\begin{gathered} D_{11}=\omega,\quad D_{12}=\mathrm{i}k,\quad D_{13}=0,\\ D_{21}=\frac{-420+140\mathrm{i}We\delta^3k^3-21(5Bo+16)\delta^2k^2-4\mathrm{i}(18Re-35\cot\theta)\delta k}{56\delta Re},\\ D_{22}=\frac{140+21(5Bo+12)\delta^2k^2+8(17\mathrm{i}k+7\omega)\delta Re}{56\delta Re},\\ D_{23}=\frac{Mak}{16Re}\left[60\mathrm{i}-\left(\mathrm{i}\omega-\frac{45}{14}k\right)\delta Re\right],\quad D_{31}=-\frac{3}{2}\mathrm{i}k,\quad D_{32}=\frac{3}{2}\mathrm{i}k,\\ D_{33}=\omega+\frac{3}{2}\mathrm{i}k+\frac{3Ma\delta k^2}{4}+\frac{\delta k^2}{Pe_s}. \end{gathered}\right\} \tag{3.3}$$

After assuming $\omega=\omega_r+\mathrm{i}\omega_i$ and setting the temporal growth rate $\omega_r=0$ in (3.2), we can obtain the neutral stability cases, where one can finally determine the critical Reynolds number as

$$Re_c=\tfrac{5}{6}\cot\theta+\tfrac{5}{2}Ma. \tag{3.4}$$

Here we note that, as long as the same scaling is adopted, equation (3.4) agrees with the result of Pereira & Kalliadasis (2008) where only the effect of surface elasticity is considered, which means that surface elasticity increases the critical Reynolds number while the existence of surface viscosity actually does not affect the instability threshold.

Meanwhile, we also solve the linear stability based on full equations (2.14)–(2.21). After linearization and assuming the disturbances of the variables in (2.14)–(2.21) to be

$$(u', v', p', \phi', h') = (\hat{u}, \hat{v}, \hat{p}, \hat{\phi}, \hat{h}) \exp(\mathrm{i}kx + \omega t) + \text{c.c.}, \tag{3.5}$$

the system is actually reduced to an ordinary differential equation eigenvalue problem, with ω being the eigenvalue. A Chebyshev spectral collocation method is employed to solve this problem, which is a well-known technique to study hydrodynamic stability (Khorrami, Malik & Ash 1989). Applying the Chebyshev spectral collocation method and upon discretization, the problem is then converted to a generalized eigenvalue problem

$$\boldsymbol{A}\boldsymbol{s} = \omega \boldsymbol{B}\boldsymbol{s}, \tag{3.6}$$

where $\boldsymbol{A}$ and $\boldsymbol{B}$ are square matrices, with $\boldsymbol{s}$ being a column vector that contains the values of $\hat{u}$, $\hat{v}$, $\hat{p}$, $\hat{\phi}$ and $\hat{h}$ at the collocation points. The computer program is based on a universal software package which has been developed by the authors to analyse hydrodynamic stability problems (Ye, Yang & Fu 2016).

Note that in experiments it is generally convenient to control the film thickness or the Reynolds number through the flow rate. Hence we introduce a set of flow parameters that only depend on the physical properties:

$$Ka = \frac{\sigma_0}{\rho g^{1/3} \upsilon^{4/3}}, \quad M = \frac{\gamma \Gamma_0}{\rho g^{1/3} \upsilon^{4/3}}, \quad Sc = \frac{\upsilon}{D_s}, \quad Bo_0 = \frac{\beta^* \Gamma_0}{\rho g^{-1/3} \upsilon^{5/3}}, \tag{3.7}$$

where Ka is the Kapitza number, M is a modified Marangoni number representing the magnitude of the surface elasticity, Sc is the Schmidt number and Bo_0 corresponds to the modified Boussinesq number characterizing the effect of surface viscosities, with $\upsilon = \mu/\rho$ denoting the kinematic viscosity of the fluid. Given $\chi = gH_N^3/\upsilon^2$ as the modified Reynolds number, equations (3.7) are related to previous parameters by

$$Re = \frac{\chi}{3}\sin\theta, \quad We = \frac{Ka}{\chi^{2/3}\sin\theta}, \quad Ma = \frac{M}{\chi^{2/3}\sin\theta}, \quad Pe_s = \frac{\chi}{3} Sc \sin\theta, \quad Bo = \frac{Bo_0}{\chi^{1/3}}. \tag{3.8a–e}$$

Figure 2 depicts the three least stable modes in the linear regime. Following the notation of Pereira & Kalliadasis (2008), they belong to the Kapitza mode due to classical long-wave instability, the concentration mode due to the diffusion and advection of surface species, and the shear mode due to the velocity profile, respectively. It is obvious that the growth rates of the concentration mode and shear mode are negative and are thus stable modes, while the Kapitza mode is unstable for small wavenumber; note that the shear mode could be unstable at some finite wavenumber when χ is very large (Pereira & Kalliadasis 2008). Moreover, the surface viscosities show a stabilizing effect on the Kapitza mode and shear mode while they slightly increase the growth rate of the concentration mode which still remains stable. Here we shall mainly focus on the Kapitza mode in the following parts since it is the only unstable mode in the long-wave region.

Figure 3 displays the influence of the surface elasticity on the film instability. Clearly, as the modified Marangoni number increases, both the growth rate and the cutoff wavenumber decrease remarkably while the wave speed increases at the same time. Moreover, as shown in figure 3(*b*), one can see that the instability threshold becomes larger and the unstable region diminishes when M increases, which shows

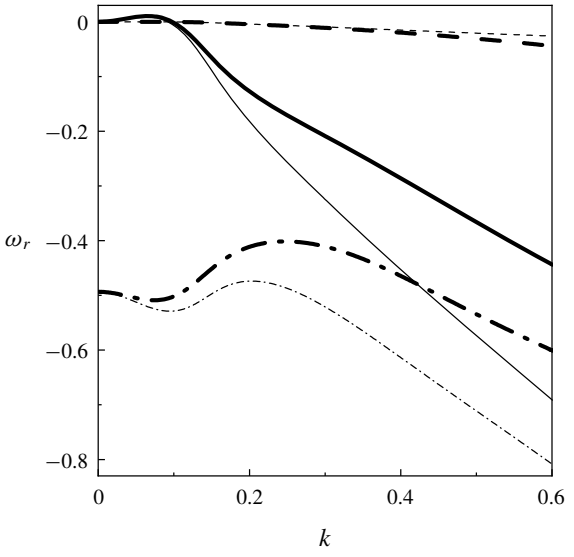

FIGURE 2. Growth rates of the three least stable modes calculated from the full equations when $\chi = 15$ and $M = 1$. The solid, dashed and dot-dashed lines correspond to the Kapitza, concentration and shear modes, respectively. Two different values of modified Boussinesq numbers are presented: $Bo_0 = 0$ for thick lines and $Bo_0 = 20$ for thin lines. Other parameters are $\theta = \pi/2$, $Ka = 3376$ and $Sc = 100$, which are fixed in the present study.

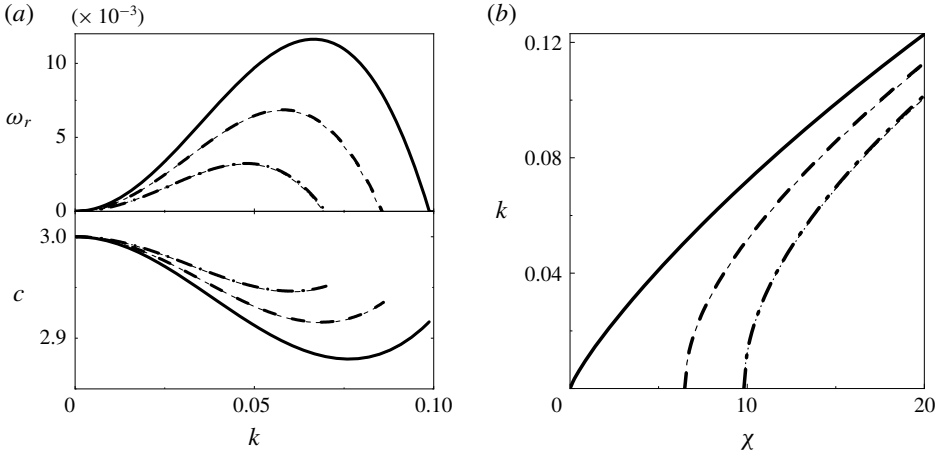

FIGURE 3. Effect of surface elasticity on the linear stability when $Bo_0 = 10$: (*a*) temporal growth rate and wave speed when $\chi = 15$, and (*b*) neutral stability curves. The solid, dashed and dot-dashed lines correspond to three modified Marangoni numbers 0, 3 and 6. Thick and thin lines represent the results of full equations and WRM, respectively (the same notation is adopted in figure 4).

a stabilizing effect of the surface elasticity on the film. In fact, a larger modified Marangoni number leads to stronger surface elasticity, which means the surface tension is more sensitive to the change of the surfactant concentration. Given the

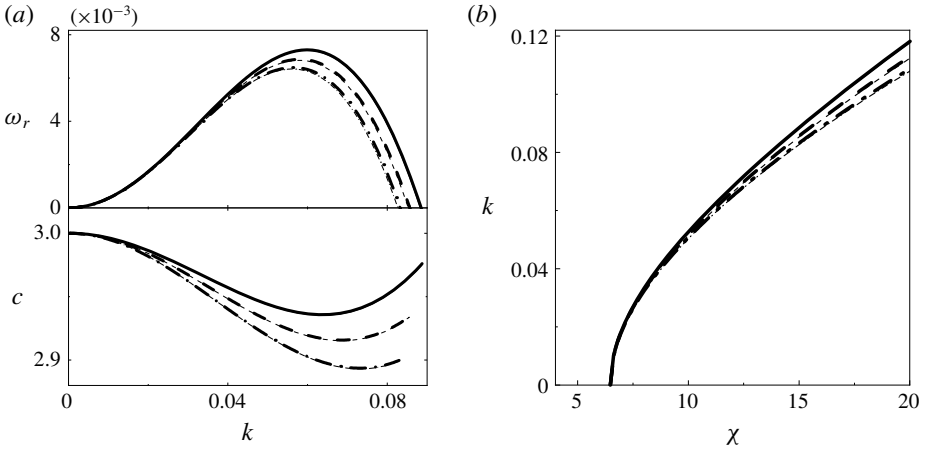

FIGURE 4. Effect of surface viscosities on the linear stability when $M = 3$: (*a*) temporal growth rate and wave speed when $\chi = 15$, and (*b*) neutral stability curves. The solid, dashed and dot-dashed lines correspond to three modified Boussinesq numbers 0, 10 and 20.

expression in (3.1) or (3.5), the small disturbances of film thickness h and surfactant concentration ϕ are in phase, which means the value of surface tension is out of phase with the film thickness in the case $M > 0$ considered here. This results in a larger value of surface tension in the troughs and a smaller value in the crests, which tends to drive the fluid flowing from the crests to the troughs, thus dampening the surface undulation and stabilizing the film.

The influence of surface viscosities is depicted in figure 4. It can be seen that the temporal growth rate, cutoff wavenumber and wave speed decrease as Bo_0 becomes larger, which implies that surface viscosities basically act to stabilize the film. However, as shown in figure 4(*b*), though the unstable region becomes smaller when Bo_0 increases, the instability threshold remains the same, which is in accordance with (3.4). Furthermore, unlike the surface elasticity, the effect of surface viscosities gradually decreases as $k \to 0$ or $Re \to Re_c$, showing almost no impact in the long-wave limit, which also supports the result that the instability threshold is not altered when the surface viscosities come into play. From figure 4 we can see that the impact of surface viscosities here is similar to that of the bulk viscosity, which attenuates the linear waves and enhances the dispersion effect, especially for wavenumbers close to the neutral value. Note that in figures 3 and 4, the results of the WRM nicely coincide with those of the full equations.

4. Travelling wave solutions

It has been observed in experiments that small initial disturbances generally evolve into travelling waves on the free surface, which propagate at a constant speed c and wave shape (Alekseenko *et al.* 1985; Liu, Gollub & Aarts 1994). In this section, we will make an effort to determine the travelling wave solutions based on the model equations (2.27)–(2.29). First we apply a coordinate transformation $\xi = x - ct$, so that (2.27) becomes

$$-ch' + q' = 0, \tag{4.1}$$

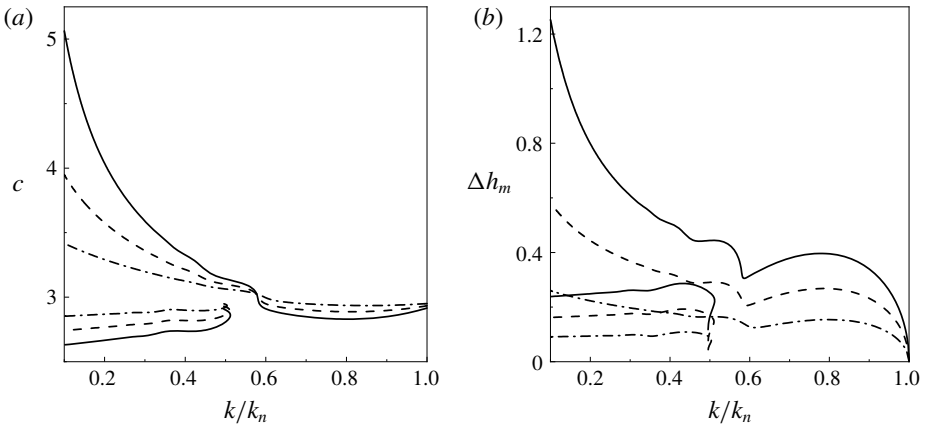

FIGURE 5. (*a*) The speed of the travelling wave and (*b*) the difference between the maximum and minimum amplitudes as functions of normalized wavenumber k/k_n at different modified Marangoni numbers when $Bo_0 = 10$ and $\chi = 15$. Solid, dashed and dot-dashed lines are for $M = 0$, $M = 3$ and $M = 6$.

where a prime represents the derivative with respect to ξ. Integrating (4.1) leads to $q = ch + q_0$ with q_0 being an integral constant. Substituting this into (2.28) and (2.29) and implementing the transformation, we have

$$A_1 h''' + A_2 h'' + A_3 \phi'' + A_4 h'^2 + A_5 h'\phi' + A_6 h' + A_7 \phi' + A_8 = 0, \tag{4.2}$$

$$B_1 \phi'' + B_2 h'' + B_3 \phi'^2 + B_4 \phi' + B_5 \phi = 0, \tag{4.3}$$

where expressions for A_1–A_8 and B_1–B_5 are given in appendix A. A closed flow condition is imposed,

$$\frac{1}{L}\int_0^L h \,\mathrm{d}\xi = 1, \tag{4.4}$$

where $L = 2\pi/k$ is the wavelength, and a phase condition, $h(0) = \phi(0) = 1$, is applied. After discretization by the Fourier spectral method, equations (4.2) and (4.3) are converted into a nonlinear algebra system, with k being a parameter. We solve this problem by the Newton–Kantorovich method together with the continuation method. An initial guess of the wave speed and profiles could be obtained from the neutral stability solutions.

Presented in figure 5 is the effect of the surface elasticity on the bifurcation diagram. The fast-wave family γ_2 emerges from the trivial solution at the cutoff wavenumber k_n through a Hopf bifurcation. The slow-wave family γ_1 originates from the γ_2 family through a period-doubling bifurcation. This bifurcation diagram is not altered when surface elasticity exists. We can see that, as the modified Marangoni number M increases, the wave speed gradually approaches that of the linear kinematic waves; and the gap $\Delta h_m = h_{max} - h_{min}$ between the maximum and minimum amplitudes is significantly reduced. Specifically, on the γ_2 branches the speed decreases remarkably when $k/k_n < 0.5$, while it slightly increases when $k/k_n > 0.6$ with M. In other words, the surface elasticity decelerates the fast-wave family, while it accelerates the slow-wave family, thus weakening the dispersion effect. This is consistent with the result of linear stability analysis in figure 3, where the Marangoni effect is shown to promote the speed of linear waves and attenuate the dispersion of the system.

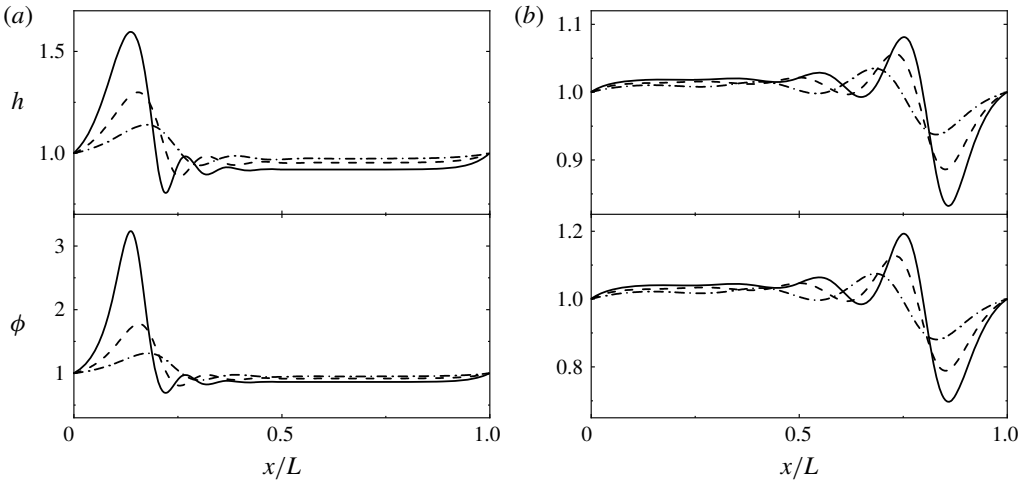

FIGURE 6. Wave profiles of film thickness h and surfactant concentration ϕ: (a) fast γ_2 family and (b) slow γ_1 family. Solid, dashed and dot-dashed lines are for $M = 0$, $M = 3$ and $M = 6$. The wavenumber is chosen to be $k = 0.02$.

Figure 6 displays the corresponding profiles of fast γ_2 waves and slow γ_1 waves of figure 5. The fast waves consist of one hump following a series of small capillary waves; the slow waves are made of one trough preceding the capillary waves. The wave shape of the surfactant concentration ϕ is similar to that of the film thickness h while its amplitude is obviously larger. For fast waves, the amplitudes of both humps and capillary ripples are dampened markedly as the surface elasticity becomes stronger. Consequently, the height of the flat portion of travelling waves is promoted due to the conservation of mass. A similar suppressing effect on the troughs and capillary waves is also observed for slow waves. Physically, the surface elasticity acts like a restoring force which resists the deformation of the free surface from the basic state.

We now explore the effect of surface elasticity on the γ_2 wave, since only the one-hump wave could be obtained during the simulation (Pumir *et al.* 1983). From figure 7 we can observe that, as the modified Reynolds number increases, both the wave speed and the maximum amplitude are promoted, showing the destabilizing effect of the inertia, which also implies that waves with large amplitude travel faster than those with small amplitude. For a given χ, both the maximum amplitude and the wave speed are reduced when the surface elasticity becomes stronger, again manifesting its stabilizing impact on the film flow.

The influence of the surface viscosities on the bifurcation diagram is demonstrated in figure 8. First we notice that the surface viscosities can modify the bifurcation behaviour of the system. Specifically, in figure 8(c,d), when Bo_0 is relatively large, the bifurcation diagram is similar to that in figure 5; whereas the opposite situation happens when the surface viscosity effect is very weak, as shown in figure 8(a,b), which is also the case when surface viscosities are absent ($Bo_0 = 0$). Similar modification of the bifurcation diagram was also identified for the effect of bulk viscous diffusion (Scheid, Ruyer-Quil & Manneville 2006). In both cases, for $k/k_n < 0.5$ (waves with typical humps or troughs), surface viscosities slightly promote the speed c and the amplitude gap Δh_m of the fast γ_2 waves; as for slow γ_1 waves, increasing the value of Bo_0 leads to a minor increase of the wave speed with a small

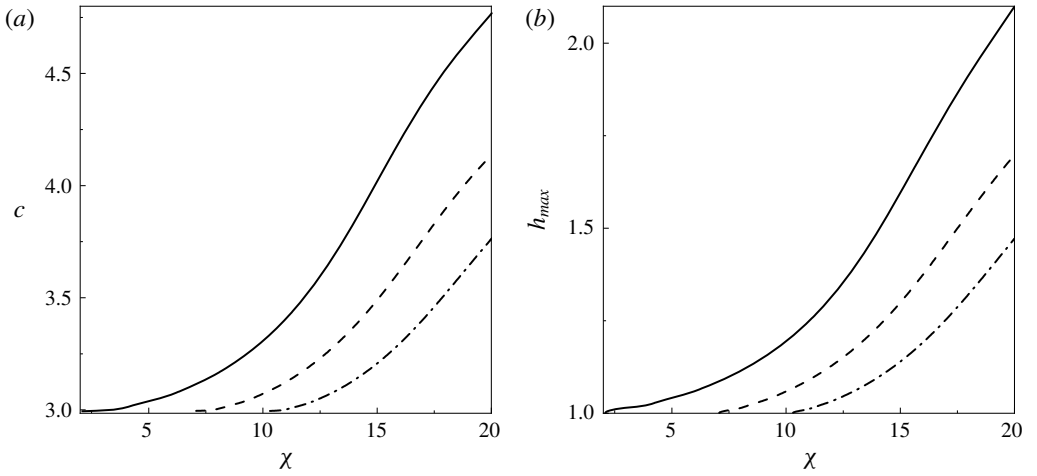

FIGURE 7. Variation of properties of γ_2 waves with modified Reynolds number χ: (*a*) speed c, and (*b*) maximum amplitude h_{max} when $Bo_0 = 10$ and $k = 0.02$. Solid, dashed and dot-dashed lines are for $M = 0$, $M = 3$ and $M = 6$.

reduction of the amplitude gap. When $k/k_n > 0.6$, the surface viscosity effect tends to decrease the wave speed and dampen the amplitude gap. Thus, we may say that surface viscosities have exerted some additional dispersion effect in the system.

Similarly, we present the wave profiles for different values of Bo_0 in figure 9. It can be seen that, for fast waves, the surface viscosity effect dampens the capillary ripples while it augments the height of the humps. On the other hand, it decreases the amplitude of troughs and amplifies that of the capillary ripples for slow waves. In fact, figures 6 and 9 both show that γ_2 waves with steeper humps travel faster while γ_1 waves with shallower troughs propagate at a lower speed.

5. Conclusions

We investigate the effect of insoluble surfactants on the stability of a thin film falling down an inclined plate and consider the case where surfactants induce both elasticity and viscosities on the free surface. The tangential and normal stress conditions are derived on the two-dimensional free surface of the film under the current Cartesian coordinate system. Both surface elasticity and viscosities are assumed to vary with the concentration of surfactants in a linear relation. The weighted residual method (WRM) is adopted to obtain a reduced model to study the film instability. In the linear analysis, it is found that the surface elasticity remarkably decreases the temporal growth rate and increases the instability threshold, showing a stabilizing role on the film instability; and though the surface viscosity effect does not modify the critical Reynolds number, it decreases the growth rate and cutoff wavenumber. The results of the WRM agree with those of the full equations satisfactorily. Travelling wave solutions are obtained from the reduced model. Surface elasticity reduces the speed of the fast-wave family while it increases that of the slow-wave family, thus damping the dispersion effect. And it suppresses the amplitude of both large-amplitude humps (troughs) and small-amplitude capillary waves, causing an effect to resist the deformation of the free surface. On the other hand, the surface viscosity effect can modify the bifurcation diagram. Moreover, it

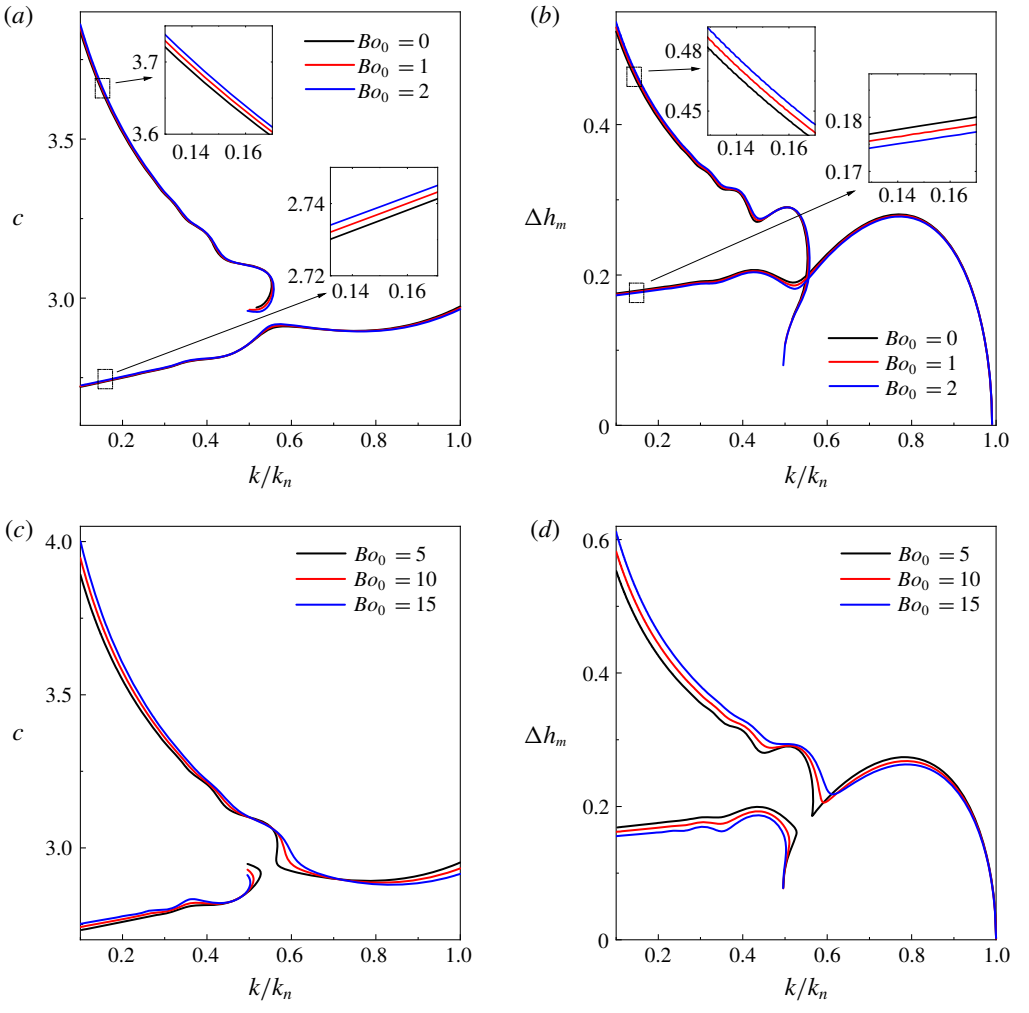

FIGURE 8. Effect of the surface viscosities on the bifurcation diagram when $M = 3$ and $\chi = 15$: (*a*,*c*) speed of the travelling waves, and (*b*,*d*) difference between maximum and minimum amplitudes.

acts to slightly increase the amplitude of the fast-wave family, decrease that of the slow-wave family and promote the wave speed of both families when the wavelengths are relatively large. Overall, surface viscosities tend to damp the linear waves, modify the bifurcation diagram and add some dispersion effect to the system, which is somewhat similar to the role of bulk viscosity.

Acknowledgements

We are grateful to the referees for their instructive comments and suggestions that improved the manuscript. This work was supported by the China's National Natural Science Funds for Distinguished Young Scholar (grant no. 11525207) and China's National Natural Science Foundation (grant nos. 11272036 and 11672025).

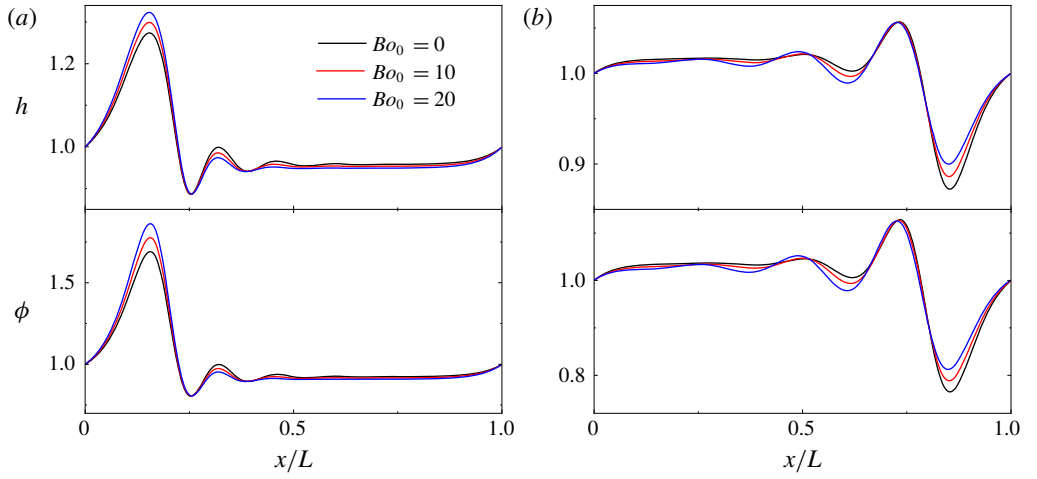

FIGURE 9. Wave profiles of film thickness h and surfactant concentration ϕ: (a) fast γ_2 family and (b) slow γ_1 family at different modified Boussinesq numbers. The wavenumber is chosen to be $k = 0.02$.

Declaration of interests

The authors report no conflict of interest.

Appendix A. Coefficients of the governing equations in a moving frame

$$\left.\begin{aligned} A_1 &= -\frac{5}{2Re}\delta^2 Weh, \quad A_2 = \frac{3\delta}{2Reh^2}\left[ch^2 + q_0\left(4h + \frac{5}{4}Bo\phi\right)\right], \\ A_3 &= -\frac{\delta Mah}{224}[45q_0 + 31ch], \quad A_4 = \frac{\delta}{2Reh^3}\left[ch^2 - q_0\left(8h + \frac{15}{2}Bo\phi\right)\right], \\ A_5 &= -\frac{\delta}{112Reh^2}[ReMa(15q_0h^2 + 34ch^3) - 210Boq_0], \\ A_6 &= \frac{1}{14Reh^2}[35\cot\theta h^3 + 2c^2Reh^2 - 2Recq_0h - 18Req_0^2], \\ A_7 &= \frac{15Ma}{4Re}, \quad A_8 = -\frac{5}{2\delta Reh^2}(h^3 - ch - q_0). \end{aligned}\right\} \tag{A 1}$$

$$\left.\begin{aligned} B_1 &= -\left(\frac{\delta}{Pe_s} + \frac{3\delta Ma}{4}h\phi\right), \quad B_2 = \left[\frac{3(ch + q_0)}{2h} - c\right]\delta^2 h'\phi, \quad B_3 = -\frac{3\delta Ma}{4}h, \\ B_4 &= \left[-\frac{3\delta Ma}{4}h'\phi + \frac{ch + 3q_0}{2h}\right], \quad B_5 = -\frac{3q_0h'}{2h^2}. \end{aligned}\right\} \tag{A 2}$$

REFERENCES

ADEBAYO, I., XIE, Z., CHE, Z. & MATAR, O. K. 2017 Doubly excited pulse waves on thin liquid films flowing down an inclined plane: an experimental and numerical study. *Phys. Rev.* E **96** (1), 013118.

ALEKSEENKO, S. V., ANTIPIN, V. A., GUZANOV, V. V., KHARLAMOV, S. M. & MARKOVICH, D. M. 2005 Three-dimensional solitary waves on falling liquid film at low Reynolds numbers. *Phys. Fluids* **17** (12), 121704.

ALEKSEENKO, S. V., NAKORYAKOV, V. E. & POKUSAEV, B. G. 1994 *Wave Flow of Liquid Films*. Begell House.

ALEKSEENKO, S. V., NAKORYAKOV, V. Y. & POKUSAEV, B. G. 1985 Wave formation on a vertical falling liquid film. *AIChE J.* **31** (9), 1446–1460.

AMAOUCHE, M., DJEMA, A. & AIT ABDERRAHMANE, H. 2012 Film flow for power-law fluids: modeling and linear stability. *Eur. J. Mech. (*B*/Fluids)* **34**, 70–84.

BENDER, A., STEPHAN, P. & GAMBARYAN-ROISMAN, T. 2017 Thin liquid films with time-dependent chemical reactions sheared by an ambient gas flow. *Phys. Rev. Fluids* **2** (8), 084002.

BENJAMIN, T. B. 1957 Wave formation in laminar flow down an inclined plane. *J. Fluid Mech.* **2**, 554–573.

BENJAMIN, T. B. 1964 Effects of surface contamination on wave formation in falling liquid films. *Arch. Mech. Stosow.* **16** (3), 615–626.

BENNEY, D. J. 1966 Long waves on liquid films. *J. Math. Phys.* **45** (1), 150–155.

BHAT, F. A. & SAMANTA, A. 2018 Linear stability of a contaminated fluid flow down a slippery inclined plane. *Phys. Rev.* E **98** (3), 033108.

BHAT, F. A. & SAMANTA, A. 2019 Linear stability analysis of a surfactant-laden shear-imposed falling film. *Phys. Fluids* **31** (5), 054103.

BLYTH, M. G. & POZRIKIDIS, C. 2004 Effect of surfactant on the stability of film flow down an inclined plane. *J. Fluid Mech.* **521**, 241–250.

CHANG, H. 1994 Wave evolution on a falling film. *Annu. Rev. Fluid Mech.* **26**, 103–136.

CHAROGIANNIS, A. & MARKIDES, C. N. 2019 Spatiotemporally resolved heat transfer measurements in falling liquid-films by simultaneous application of planar laser-induced fluorescence (PLIF), particle tracking velocimetry (PTV) and infrared (IR) thermography. *Exp. Therm. Fluid Sci.* **107**, 169–191.

CHAROGIANNIS, A., DENNER, F., VAN WACHEM, B. G. M., KALLIADASIS, S. & MARKIDES, C. N. 2017 Detailed hydrodynamic characterization of harmonically excited falling-film flows: a combined experimental and computational study. *Phys. Rev. Fluids* **2** (1), 014002.

CRASTER, R. V. & MATAR, O. K. 2009 Dynamics and stability of thin liquid films. *Rev. Mod. Phys.* **81** (3), 1131–1198.

D'ALESSIO, S. J. D. & PASCAL, J. P. 2016 Thermosolutal Marangoni effects on the inclined flow of a binary liquid with variable density. II. Nonlinear analysis and simulations. *Phys. Rev. Fluids* **1** (8), 083604.

DÁVALOS-OROZCO, L. A. 2012 The effect of the thermal conductivity and thickness of the wall on the nonlinear instability of a thin film flowing down an incline. *Intl J. Non-Linear Mech.* **47** (4), 1–7.

DING, Z. & WONG, T. N. 2015 Falling liquid films on a slippery substrate with Marangoni effects. *Intl J. Heat Mass Transfer* **90**, 689–701.

ELLABAN, E., PASCAL, J. P. & D'ALESSIO, S. J. D. 2017 Instability of a binary liquid film flowing down a slippery heated plate. *Phys. Fluids* **29** (9), 092105.

EMMERT, R. E. 1954 A study of gas absorption in falling liquid films. *Chem. Engng Prog.* **50** (2), 87–93.

FU, Q. F., HU, T. & YANG, L. J. 2018 Instability of a weakly viscoelastic film flowing down a heated inclined plane. *Phys. Fluids* **30** (8), 084102.

GEORGANTAKI, A., VLACHOGIANNIS, M. & BONTOZOGLOU, V. 2012 The effect of soluble surfactants on liquid film flow. *J. Phys. Conf. Ser.* **395** (1), 012165.

GEORGANTAKI, A., VLACHOGIANNIS, M. & BONTOZOGLOU, V. 2016 Measurements of the stabilisation of liquid film flow by the soluble surfactant sodium dodecyl sulfate (SDS). *Intl J. Multiphase Flow* **86**, 28–34.

JI, W. & SETTERWALL, F. 1994 On the instabilities of vertical falling liquid films in the presence of surface-active solute. *J. Fluid Mech.* **278**, 297–323.

JOO, S. W., DAVIS, S. H. & BANKOFF, S. G. 1991 Long-wave instabilities of heated falling films: two-dimensional theory of uniform layers. *J. Fluid Mech.* **230**, 117–146.

KAPITZA, P. L. & KAPITZA, S. P. 1949 Wave flow of thin viscous liquid films. *Zh. Eksp. Teor. Fiz.* **19**, 105–120.

KARAPETSAS, G. & BONTOZOGLOU, V. 2014 The role of surfactants on the mechanism of the long-wave instability in liquid film flows. *J. Fluid Mech.* **741**, 139–155.

KHARLAMOV, S. M., GUZANOV, V. V., BOBYLEV, A. V., ALEKSEENKO, S. V. & MARKOVICH, D. M. 2015 The transition from two-dimensional to three-dimensional waves in falling liquid films: wave patterns and transverse redistribution of local flow rates. *Phys. Fluids* **27** (11), 114106.

KHORRAMI, M. R., MALIK, M. R. & ASH, R. L. 1989 Application of spectral collocation techniques to the stability of swirling flows. *J. Comput. Phys.* **81** (1), 206–229.

LIN, S. P. 1974 Finite amplitude side-band stability of a viscous film. *J. Fluid Mech.* **63**, 417–429.

LIU, J., GOLLUB, J. P. & AARTS, D. G. 1994 Solitary wave dynamics of film flows. *Phys. Fluids* **6** (5), 1702–1712.

LIU, J., PAUL, J. D. & GOLLUB, J. P. 1993 Measurements of the primary instabilities of film flows. *J. Fluid Mech.* **250**, 69–101.

LIU, J., SCHNEIDER, J. B. & GOLLUB, J. P. 1995 Three-dimensional instabilities of film flows. *Phys. Fluids* **7** (1), 55–67.

MARTÍNEZ-CALVO, A. & SEVILLA, A. 2018 Temporal stability of free liquid threads with surface viscoelasticity. *J. Fluid Mech.* **846**, 877–901.

OGDEN, K., PASCAL, J. & D'ALESSIO, S. 2011 Gravity-driven flow over heated, porous, wavy surfaces. *Phys. Fluids* **23** (12), 122102.

ORON, A. & EDWARDS, D. A. 1993 Stability of a falling liquid film in the presence of interfacial viscous stress. *Phys. Fluids* A **5** (2), 506–508.

ORON, A., DAVIS, S. H. & BANKOFF, S. G. 1997 Long-scale evolution of thin liquid films. *Rev. Mod. Phys.* **69** (3), 931–980.

PASCAL, J. P., D'ALESSIO, S. J. D. & ELLABAN, E. 2019 Stability of inclined flow of a liquid film with soluble surfactants and variable mass density. *Phys. Rev. Fluids* **4** (5), 054004.

PEREIRA, A. & KALLIADASIS, S. 2008 Dynamics of a falling film with solutal Marangoni effect. *Phys. Rev.* E **78** (3), 036312.

PONCE-TORRES, A., MONTANERO, J. M., HERRADA, M. A., VEGA, E. J. & VEGA, J. M. 2017 Influence of the surface viscosity on the breakup of a surfactant-laden drop. *Phys. Rev. Lett.* **118** (2), 024501.

PUMIR, A., MANNEVILLE, P. & POMEAU, Y. 1983 On solitary waves running down an inclined plane. *J. Fluid Mech.* **135**, 27–50.

RUYER-QUIL, C. & MANNEVILLE, P. 2000 Improved modeling of flows down inclined planes. *Eur. Phys. J.* B **15** (2), 357–369.

RUYER-QUIL, C. & MANNEVILLE, P. 2002 Further accuracy and convergence results on the modeling of flows down inclined planes by weighted-residual approximations. *Phys. Fluids* **14** (1), 170–183.

RUYER-QUIL, C., CHAKRABORTY, S. & DANDAPAT, B. S. 2012 Wavy regime of a power-law film flow. *J. Fluid Mech.* **692**, 220–256.

RUYER-QUIL, C., KOFMAN, N., CHASSEUR, D. & MERGUI, S. 2014 Dynamics of falling liquid films. *Eur. Phys. J.* E **37** (4), 30.

SADIQ, I. M. R. & USHA, R. 2008 Thin Newtonian film flow down a porous inclined plane: stability analysis. *Phys. Fluids* **20** (2), 022105.

SALVAGNINI, W. M. & TAQUEDA, M. E. S. 2004 A falling-film evaporator with film promoters. *Ind. Engng Chem. Res.* **43** (21), 6832–6835.

SAMANTA, A. 2008 Stability of liquid film falling down a vertical non-uniformly heated wall. *Physica* D **237** (20), 2587–2598.

SAMANTA, A., RUYER-QUIL, C. & GOYEAU, B. 2011 A falling film down a slippery inclined plane. *J. Fluid Mech.* **684**, 353–383.

SCHEID, B., RUYER-QUIL, C. & MANNEVILLE, P. 2006 Wave patterns in film flows: modelling and three-dimensional waves. *J. Fluid Mech.* **562**, 183–222.

SCHEID, B., RUYER-QUIL, C., THIELE, U., KABOV, O. A., LEGROS, J. C. & COLINET, P. 2005 Validity domain of the Benney equation including the Marangoni effect for closed and open flows. *J. Fluid Mech.* **527**, 303–335.

SCRIVEN, L. E. & STERNLING, C. V. 1960 The Marangoni effects. *Nature* **187** (4733), 186–188.

SHINE, S. R. & NIDHI, S. S. 2018 Review on film cooling of liquid rocket engines. *Propul. Power Res.* **7** (1), 1–18.

SHKADOV, V. Y. 1967 Wave flow regimes of a thin layer of viscous fluid subject to gravity. *Izv. Akad. Nauk SSSR Mekh. Zhidk. Gaza* **2** (1), 43–51.

SMITH, M. K. 1990 The mechanism for the long-wave instability in thin liquid films. *J. Fluid Mech.* **217**, 469–485.

SQUIRES, T. M. & QUAKE, S. R. 2005 Microfluidics: fluid physics at the nanoliter scale. *Rev. Mod. Phys.* **77** (3), 977–1026.

STIRBA, C. & HURT, D. M. 1955 Turbulence in falling liquid films. *AIChE J.* **1** (2), 178–184.

TAILBY, S. R. & PORTALSKI, S. 1961 The optimum concentration of surface active agents for the suppression of ripples. *Trans. Inst. Chem.* **39**, 328–336.

TREVELYAN, P., SCHEID, B., RUYER-QUIL, C. & KALLIADASIS, S. 2007 Heated falling films. *J. Fluid Mech.* **592**, 295–334.

WEINSTEIN, S. J. & RUSCHAK, K. J. 2004 Coating flows. *Annu. Rev. Fluid Mech.* **36**, 29–53.

WHITAKER, S. 1964 Effect of surface active agents on the stability of falling liquid films. *Ind. Engng Chem. Fundam.* **3** (2), 132–142.

YE, H. Y., YANG, L. J. & FU, Q. F. 2016 Spatial instability of viscous double-layer liquid sheets. *Phys. Fluids* **28** (10), 102101.

YIH, C. S. 1963 Stability of liquid flow down an inclined plane. *Phys. Fluids* **6** (3), 321–334.